PAPER

Relative Patlak plot for dynamic PET parametric imaging without the need for early-time input function

IOP Publishing Phys. Med. Biol. 63 (2018) 165004 (12pp) https://doi.org/10.1088/1361-6560/aad444

Physics in Medicine & Biology

IPEM Institute of Physics and Engineering in Medicine

RECEIVED
19 February 2018

REVISED
14 July 2018

ACCEPTED FOR PUBLICATION
18 July 2018

PUBLISHED
10 August 2018

PAPER

Relative Patlak plot for dynamic PET parametric imaging without the need for early-time input function

Yang Zuo[1], Jinyi Qi[2] and Guobao Wang[1,3]

[1] Department of Radiology, University of California at Davis, Sacramento, CA 95817, United States of America
[2] Department of Biomedical Engineering, University of California at Davis, Davis, CA 95616, United States of America
[3] Comprehensive Cancer Center, University of California at Davis, Sacramento, CA 95817, United States of America

E-mail: gbwang@ucdavis.edu

Keywords: dynamic PET, kinetic modeling, Patlak plot, parametric imaging

Abstract

The Patlak graphical method is widely used in parametric imaging for modeling irreversible radiotracer kinetics in dynamic PET. The net influx rate of radiotracer can be determined from the slope of the Patlak plot. The implementation of the standard Patlak method requires the knowledge of full-time input function from the injection time until the scan end time, which presents a challenge for use in the clinic. This paper proposes a new relative Patlak plot method that does not require early-time input function and therefore can be more efficient for parametric imaging. Theoretical analysis proves that the effect of early-time input function is a constant scaling factor on the Patlak slope estimation. Thus, the parametric image of the slope of the relative Patlak plot is related to the parametric image of standard Patlak slope by a global scaling factor. This theoretical finding has been further demonstrated by computer simulation and real patient data. The study indicates that parametric imaging of the relative Patlak slope can be used as a substitute of parametric imaging of standard Patlak slope for tasks that do not require absolute quantification, such as lesion detection and tumor volume segmentation.

1. Introduction

Dynamic positron emission tomography (PET) provides four-dimensional distribution (three-dimensional space plus one-dimentional time) of radiotracer in living body and is attracting more and more research interests (Schmidt and Turkheimer 2002, Rahmim *et al* 2009, Wang and Qi 2013, Reader and Verhaeghe 2014). Analyzing dynamic PET data relies on kinetic modeling which commonly uses a temporal model to describe the kinetics of radiotracer uptake (Schmidt and Turkheimer 2002). Voxel-wise implementation of kinetic modeling provides parametric maps of kinetic parameters indicating the biological characters of the tissue (Gunn *et al* 1998). Parametric imaging has been found useful in many applications including tumor detection (Kordower *et al* 2000, Gill *et al* 2003) and extraction of metabolic tumor volume (Visser *et al* 2008).

The Patlak graphical plot is a widely used kinetic analysis method in dynamic PET for extracting the net influx rate of irreversible uptake of a radiotracer (Patlak *et al* 1983, Patlak and Blasberg 1985, Choi *et al* 1991, Choi *et al* 1993, Gambhir *et al* 1989). It is also used for kinetic modeling in dynamic magnetic resonance imaging (MRI) (Hackstein *et al* 2003) and computed tomography (CT) (Miles *et al* 1999, Hackstein *et al* 2004, Hom *et al* 2009). Compared with nonlinear compartmental modeling, the Patlak method uses a linear model and has the advantage of being computationally efficient for parametric imaging and being easier to be implemented into new reconstruction methods (Tsoumpas *et al* 2008, Wang *et al* 2008, Tang *et al* 2010, Angelis *et al* 2011, Zhu *et al* 2014) and for whole-body imaging (Zhu *et al* 2014, Karakatsanis *et al* 2015, 2016, Hu *et al* 2017).

Input function is essential for tracer kinetic modeling. Although the Patlak graphical plot only examines the time points of tissue activity at steady state, the standard Patlak method requires the knowledge of full-time input function from the radiotracer injection time until the dynamic scan end time. To obtain the information of full-time input function, either many blood samples are needed if arterial blood sampling is used or a long scan covering early-time points is required if the image-derived or reference region input function is used. For example

in dynamic ^{18}F-FDG PET imaging, an 1 h dynamic scan is required to derive the full blood input function from dynamic images, though only late 20–30 min are actually used to extract the tracer activity of tissue. This requirement for early-time input function presents a challenge for applying the Patlak method in the clinic, particularly for whole-body imaging (Hu *et al* 2017).

This paper proposes a new relative Patlak plot method for PET parametric imaging. Compared with the standard Patlak plot, the proposed relative plot does not require the information of early-time input function. Mathematical analysis is used to show the relationship between the slope of the new plot and that of the standard Patlak plot. The theoretical findings are further validated by computer simulation of dynamic PET data and real patient scan data.

2. Theory

2.1. Standard Patlak plot

Let us denote the radiotracer concentration at time t in a tissue region of interest (ROI) or voxel by $C_T(t)$ and tracer concentration in the plasma by $C_P(t)$. The Patlak plot exploits the linearity between the normalized tissue concentration and normalized integral of input function $C_P(t)$ after a steady-state time t^*. Mathematically, it is described by a linear equation:

$$\frac{C_T(t)}{C_P(t)} = K_i \cdot \frac{\int_0^t C_P(\tau)d\tau}{C_P(t)} + b \quad (t > t^*), \tag{1}$$

where K_i is the slope constant that represents the net influx rate of irreversible uptake of a radiotracer and b is the intercept which equivalently indicates blood volume in the tissue and the normalized tracer concentration from reversible compartments.

By acquiring dynamic PET data for multiple time frames, one can plot the data of

$$y(t) = \frac{C_T(t)}{C_P(t)} \tag{2}$$

and

$$x(t) = \frac{\int_0^t C_P(\tau)d\tau}{C_P(t)} \tag{3}$$

of each time frame and fit the data points using the linear model equation (1). The slope K_i and intercept b are then estimated by the linear regression. Note that although $y(t)$ is only sampled for $t > t^*$, $x(t)$ contains the integral of the input function $C_P(t)$ from the injection time $t = 0$ till the scan end time. Thus the full-time input function needs to be known for the standard Patlak plot.

Given a set of measurements at M time points $\{t_m\}_{m=1}^M$ with $t_1 = t^*$ and t_m denoting the midpoint of each time frame, the Patlak slope and intercept can be estimated using the following least-squares formulation:

$$\hat{K}_i, \hat{b} = \arg\min_{K_i,b} \sum_{m=1}^{M} [y(t_m) - K_i \cdot x(t_m) - b]^2 \tag{4}$$

where the integration in $x(t)$ is calculated using the rectangle rule

$$x(t_m) = \frac{\sum_{n=1}^{m} C_P(t_n)\Delta t_n}{C_P(t_m)},$$

with Δt_n denoting the scan duration for nth frame. The optimal solution has the following analytic formula:

$$\hat{K}_i = \frac{V(x,y)}{V(x,x)}, \tag{5}$$

$$\hat{b} = \bar{y} - \hat{K}_i \cdot \bar{x}, \tag{6}$$

where $V(\cdot,\cdot)$ and $\bar{\cdot}$ have the forms as follows:

$$\bar{x} = \frac{1}{M}\sum_{m=1}^{M} x(t_m), \tag{7}$$

$$V(x,y) = \frac{1}{M}\sum_{m=1}^{M} x(t_m)y(t_m) - \bar{x}\cdot\bar{y}, \tag{8}$$

which correspond to the mean and covariance if x and y are considered as random variables.

2.2. Proposed relative Patlak plot

We propose a new relative Patlak plot which has the following model equation:

$$\frac{C_T(t)}{C_P(t)} = K_i' \cdot \frac{\int_{t^*}^{t} C_P(\tau)d\tau}{C_P(t)} + b' \quad (t > t^*), \tag{9}$$

where K_i' and b' are the slope and intercept of the new plot, respectively.

The new relative Patlak method plots the data of $y(t)$ in equation (2) versus

$$x'(t) = \frac{\int_{t^*}^{t} C_P(\tau)d\tau}{C_P(t)} \tag{10}$$

to get the slope K_i' and intercept b'. This new model is very similar to the standard Patlak plot equation, except that the integral of the input function $C_P(t)$ here is from t^* to t, not from 0 to t. The integral of $C_P(t)$ over early time from 0 to t^* is no longer needed in this new plot.

Similarly to the least-squares estimation for the standard Patlak plot, the slope and intercept of the relative Patlak plot can be estimated by

$$\hat{K}_i', \hat{b}' = \arg\min_{K_i', b'} \sum_{m=1}^{M} [y(t_m) - K_i' \cdot x'(t_m) - b']^2, \tag{11}$$

which gives the following optimal solution:

$$\hat{K}_i' = \frac{V(x', y)}{V(x', x')}, \tag{12}$$

$$\hat{b}' = \bar{y} - \hat{K}_i' \cdot \bar{x}' \tag{13}$$

where $\bar{\cdot}$ and $V(\cdot,\cdot)$ are defined in equations (7) and (8), respectively.

2.3. Theoretical relation between the two plots

The new relative Patlak plot is closely related to the standard Patlak plot. Here we examine the theoretical relation between the two plots using analytical derivations. Let us define

$$x^0(t) = \frac{\int_{0}^{t^*} C_P(\tau)d\tau}{C_P(t)} \tag{14}$$

to account for the component of early-time input function which appears in $x(t)$ but not in $x'(t)$. Obviously, we have

$$x(t) = x^0(t) + x'(t). \tag{15}$$

In dynamic PET scans, the late-time input function $C_P(t)$ for $t > t^*$ can be analytically expressed by an exponential function:

$$C_P(t) = a_1 \cdot e^{-a_2 t}, \tag{16}$$

where $a_1, a_2 > 0$. For example, the widely used Feng model for dynamic ^{18}F-FDG PET has the form (Feng *et al* 1993)

$$C_P(t) = (A_1 t - A_2 - A_3)e^{-L_1 t} + A_2 e^{-L_2 t} + A_3 e^{-L_3 t}, \tag{17}$$

with the following parameters $A_1 = 851.1\,\text{mg/100 ml min}^{-1}$, $A_2 = 21.9\,\text{mg/100 ml}$, $A_3 = 20.8\,\text{mg/100 ml}$, $L_1 = 4.1\,\text{min}^{-1}$, $L_2 = 0.12\,\text{min}^{-1}$, $L_3 = 0.01\,\text{min}^{-1}$. For $t > t^* = 30\,\text{min}$, the Feng input function is dominated by the term $A_3 e^{-L_3 t}$ while the other two terms are negligible. Another example is the reference tissue input in dynamic ^{11}C-PIB PET, where the tail also approximately follows an exponential function (Zhou *et al* 2012).

As a result, $x^0(t)$ and $x'(t)$ can be rewritten as

$$x^0(t) = \frac{s^*}{a_1} e^{a_2 t}, \tag{18}$$

$$x'(t) = \frac{1}{a_2}\left(e^{-a_2(t^* - t)} - 1\right), \tag{19}$$

with s^* being the integral of blood input over the early time from time 0 to t^*,

$$s^* = \int_0^{t^*} C_P(\tau)d\tau. \tag{20}$$

It is then not difficult to verify the following linear relationship between $x^0(t)$ and $x'(t)$:

$$x^0(t) = \alpha + \beta x'(t) \tag{21}$$

where α and β are both constants that only depend on t^*:

$$\alpha = \frac{1}{a_1} s^* e^{a_2 t^*}, \tag{22}$$

$$\beta = \frac{a_2}{a_1} s^* e^{a_2 t^*}. \tag{23}$$

Using equation (15), the standard Patlak plot model equation (1) can be re-written as

$$y(t) = K_i \cdot [x'(t) + x^0(t)] + b. \tag{24}$$

Substituting equation (21) into equation (24), we obtain the following equivalence:

$$y(t) = (1+\beta)K_i \cdot x'(t) + (\alpha K_i + b), \tag{25}$$

$$= K_i' x'(t) + b' \tag{26}$$

with

$$K_i' = (1+\beta)K_i, \tag{27}$$

$$b' = b + \alpha K_i. \tag{28}$$

The two equations above indicate that the relative Patlak slope K_i' is proportional to the standard Patlak slope K_i with a scaling factor $(1+\beta)$. The intercept of the relative Patlak plot is equivalent to the intercept of the standard Patlak plot plus a shift αK_i.

The scaling factor $(1+\beta)$ only depends on the input function and is independent of tissue time activity. It is therefore a global scaling factor when the Patlak plot is implemented for parametric imaging. Thus, the parametric image of the relative Patlak slope K_i' is equivalent to the parametric image of the standard Patlak slope K_i up to a scaling factor.

2.4. Theoretical relation between the least squares estimates

In practice, the slope and intercept of a graphical plot are commonly estimated by a least squares optimization. Here we examine the theoretical relation between the standard Patlak and relative Patlak least squares estimates.

Based on equation (21), $x(t)$ and $x'(t)$ approximately satisfy a linear relation:

$$x(t) = \nu + S \cdot x'(t) \quad (t > t^*), \tag{29}$$

where S and ν are respectively equivalent to $(1+\beta)$ and α if the late-time blood input is described by an exponential function. Alternatively, S and ν can be estimated by a linear regression without assuming an exponential model:

$$S = \frac{V(x', x)}{V(x', x')}, \tag{30}$$

$$\nu = \bar{x} - S \cdot \bar{x}'. \tag{31}$$

Substituting equation (29) into the least squares estimate of the standard Patlak slope $\hat{K}_i$ in equation (5) leads to the following expression:

$$\hat{K}_i = \frac{V(\nu + Sx', y)}{V(\nu + Sx', \nu + Sx')}. \tag{32}$$

Note that the function $V(\cdot, \cdot)$ has the following properties:

$$V(x, y) = V(y, x), \tag{33}$$

$$V(c \cdot x, y) = c \cdot V(x, y), \tag{34}$$

$$V(x + c, y) = V(x, y), \tag{35}$$

where c is an arbitrary constant. Using these properties and the definition of the least-squares estimate of the relative Patlak slope $\hat{K}'_i$ defined in equation (12), we then obtain the scaling relation between $\hat{K}'_i$ and $\hat{K}_i$:

$$\hat{K}'_i = S \cdot \hat{K}_i. \tag{36}$$

We can also derive the following relation between the least-squares estimates of the two intercepts $\hat{b}'$ and $\hat{b}$:

$$\hat{b}' = \hat{b} + \nu \cdot \hat{K}_i. \tag{37}$$

These results indicate that the theoretical relation between the standard Patlak plot and relative Patlak plot holds true as long as $x(t)$ and $x'(t)$ satisfy the linear relationship given in equation (29) regardless of the shape of the blood input function.

3. Materials and methods

3.1. Validation using computer simulation

We first conducted a computer simulation to validate the theoretical results on the scaling relationship between the standard Patlak slope and relative Patlak slope. This simulation study was designed for mimicking parametric imaging where a single blood input function is used and different voxels share the same scaling factor between the standard Patlak slope and relative Patlak slope. One-hour dynamic ^{18}F-FDG scan was simulated following the scanning sequence of a total of 55 frames: 30 × 10 s frames, 10 × 60 s frames and 15 × 180 s frames. The blood input function in this simulation was generated using the analytical Feng model (Feng *et al* 1993). Following the standard two-tissue compartmental model, we simulated 10 000 groups of random kinetic parameters which follow a Gaussian distribution with the mean of kinetic parameters being $K_1 = 0.81$ ml/ml/min, $k_2 = 0.38\,\text{min}^{-1}$, $k_3 = 0.1\,\text{min}^{-1}$, $k_4 = 0\,\text{min}^{-1}$ and standard deviation being 40% of the mean kinetic parameters. Noise-free time activity curves (TACs) were generated with the simulated FDG kinetics and blood input function. Zero-mean Gaussian noise were then added to each noise-free TAC $\{c_m\}_{m+1}^{M}$ using the noise standard deviation (Wu and Carson 2002) defined by

$$SD_m = S_c \cdot \sqrt{c_m \exp(\lambda t_m)/\Delta t_m}, \tag{38}$$

where S_c is a scaling factor to adjust SD to match with realistic dynamic FDG-PET data at different noise levels. $S_c = 1.0$ was used to simulate a voxel-level high noise in this simulation. λ is the decay constant of the radiotracer set to be $\ln(2)/T_{1/2}$ with $T_{1/2} = 109.8$ min. Δt_m is the scan duration of time frame m and t_m is the middle time of frame m.

To demonstrate the wide applicability of the method, we conducted a second simulation study to examine if a bi-exponential input model $C_P(t) = a_1 e^{-a_2 t} + b_1 e^{-b_2 t}$ meets the linear relation between $x(t)$ and $x'(t)$. The scanning sequence was the same as used in the first simulation study. To mimic blood input functions of different tail shape, one thousand sets of the model parameters were randomly generated using the uniform distribution with the intervals $a_1 \in [0, 50]$, $b_1 \in [0, 50]$, $a_2 \in [0, 1]$, $b_2 \in [0, 1]$. The parameter bounds are projected from the Feng input model. The coefficient of the Pearson correlation between $x(t)$ and $x'(t)$ was calculated for each realization of the input function.

3.2. Validation using patient scans

We further validated the theoretical results using dynamic FDG-PET scans of two human patients, one with breast cancer and the other with coronary heart disease.

The breast patient scan was operated on the GE Discovery 690 PET/CT scanner at UC Davis Medical Center. The patient received 5 mCi ^{18}F-FDG with a bolus injection. List-mode time-of-flight data acquisition commenced right after the FDG injection and lasted for 60 min. A low-dose transmission CT scan was then performed at the end of PET scan to provide CT image for PET attenuation correction. The raw data were then binned into a total of 49 dynamic frames: 30 × 10 s, 10 × 60 s and 9 × 300 s. Dynamic PET images were reconstructed using the standard ordered subsets expectation maximization (OSEM) algorithm with 2 iterations and 32 subsets as provided in the vendor software. All data corrections including normalization, attenuation correction, scattered correction and randoms correction, were included in the reconstruction process. A region of interest was placed in the left ventricle region to extract blood input function.

The cardiac scan was performed on the GE Discovery ST PET/CT scanner at UC Davis Medical Center in two-dimensional mode. The scanner has no time-of-flight capability. The patient received 20 mCi ^{18}F-FDG with a bolus injection. List-mode data acquisition commenced right after the FDG injection and lasted for 60 min. A low-dose transmission CT scan was then performed at the end of PET scan to provide CT image for PET attenuation correction. The raw data were binned into a total of 49 dynamic frames: 30 × 10 s, 10 × 60 s and 9 × 300 s. Dynamic PET images were reconstructed using the standard ordered subsets expectation maximization (OSEM) algorithm with 2 iterations and 30 subsets as provided in the vendor software. All data corrections including

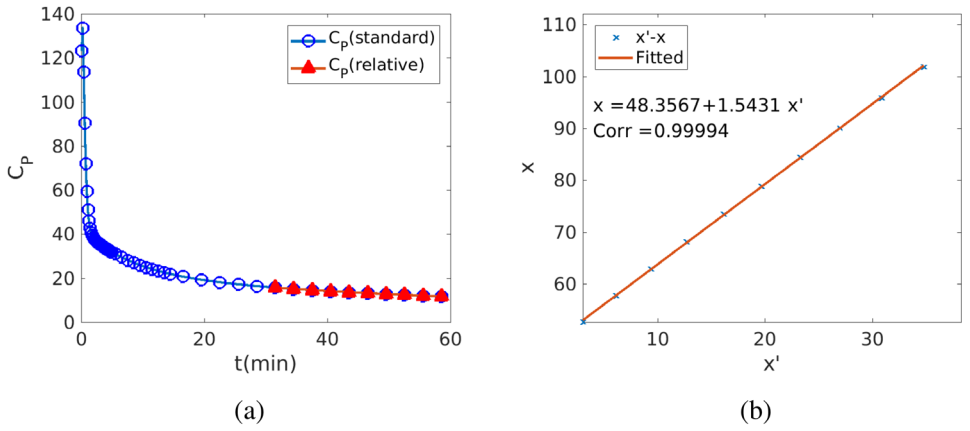

Figure 1. Blood input functions in the simulation. (a) Full-time blood input function (circles) by the Feng model for the Standard Patlak and late time points (solid triangles) for the relative Patlak; (b) linear relation between x and x' with $t^* = 30$ min.

normalization, attenuation correction, scattered correction and randoms correction, were included in the reconstruction process. The blood input function was also extracted from the left ventricle region.

4. Results

4.1. Simulation results

The simulated noisy TACs based on the Feng input model were first analyzed using the standard Patlak plot and new relative Patlak plot with a start time $t^* = 30$ min. For the standard Patlak plot, the full-time blood input from 0 to 60 min was used to estimate the slope K_i. For the relative Patlak plot, only the input function after t^* was used to estimate the slope K_i'. Early-time input function is not needed for the relative Patlak plot, which is equivalent to setting those time points to zeros. The two input functions are graphically compared in figure 1(a). We then verified the linear relation between $x(t) = (\int_0^t C_P(\tau)d\tau)/C_P(t)$ and $x'(t) = (\int_{t^*}^t C_P(\tau)d\tau)/C_P(t)$ with $t > t^*$. Figure 1(b) shows the plot of $x(t)$ versus $x'(t)$ for the simulated Feng input function. The linear fit was excellent with a pairwise linear correlation coefficient close to 1.

Examples of the the standard Patlak plot and relative Patlak plot are shown in figures 2(a) and (b). We examined the linearity between the standard Patlak slope K_i and the relative Patlak slope K_i'. Figure 3(a) shows the estimated K_i' versus K_i values for all the simulated 10 000 TACs. The correlation coefficient between K_i' and K_i was 1.0, indicating a perfect linearity. The intercept is negligible, indicating K_i' values are equal to K_i values times the scaling factor. The slope of the linear plot of K_i' versus K_i is approximately equal to the slope of the linear plot of $x(t)$ versus $x'(t)$. The relation between K_i' and K_i is therefore verified by the simulation data. Figure 3(b) further shows that the correlation coefficient between K_i' and K_i remains stable and close to 1 when t^* varied from 10 min to 54 min, though the scaling factor between them depends on t^*. Note that t^* could not be greater than 54 min given the defined time frames, otherwise less than two time points could be used for the Patlak plots.

Figure 4(a) shows all the correlation coefficients of $x'(t)$ versus $x(t)$ for 1000 random realizations of the bio-exponential input function. Figure 4(b) show the correlation plot of $x'(t)$ versus $x(t)$ for a specific model parameter set $a_1 = 36.288, a_2 = 0.093, b_1 = 1.543, b_2 = 0.001$, which corresponds to the the sample point in figure 4(a) with the lowest correlation coefficient $R = 0.9927$. The results validate the wide applicability of the assumption (equation (29)) we made for establishing the relation between the relative Patlak slope and standard Patlak slope.

4.2. Patient results

4.2.1. Blood input functions

The image-derived input functions from the breast patient scan and cardiac patient scan are shown in figures 5(a) and (b), respectively. The start time t^* was initially set to 30 min. Figure 6 validates that the late-time time points of the two blood input functions approximately follow a mono-exponential model $C_P(t) = a_1 e^{-a_2 t}$ for $t \geqslant t^*$. It is not surprising that higher noise presents in the cardiac patient data because the scan was operated in a 2D mode and also without time-of-flight capability.

The linear relation between $x(t)$ and $x'(t)$ after $t^* = 30$ min is shown in figure 7(a) for the breast patient data and in figure 7(b) for the cardiac patient data.

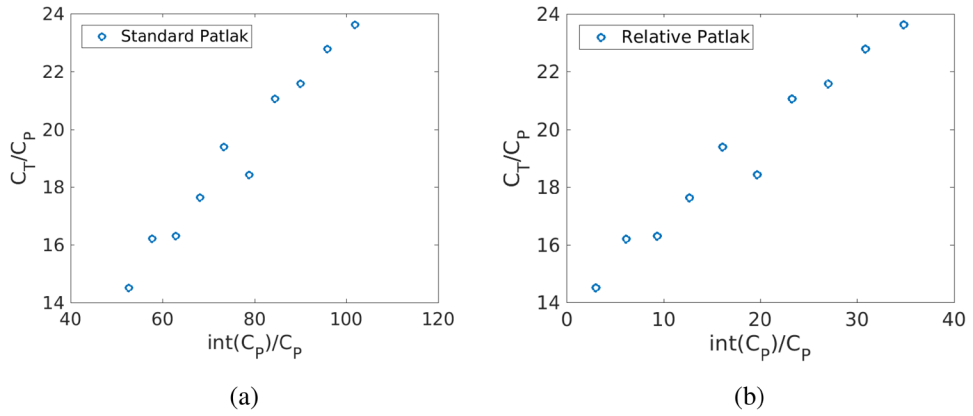

Figure 2. Comparison of the standard Patlak plot and relative Patlak plot in the simulation. (a) Standard Patlak plot; (b) relative Patlak plot.

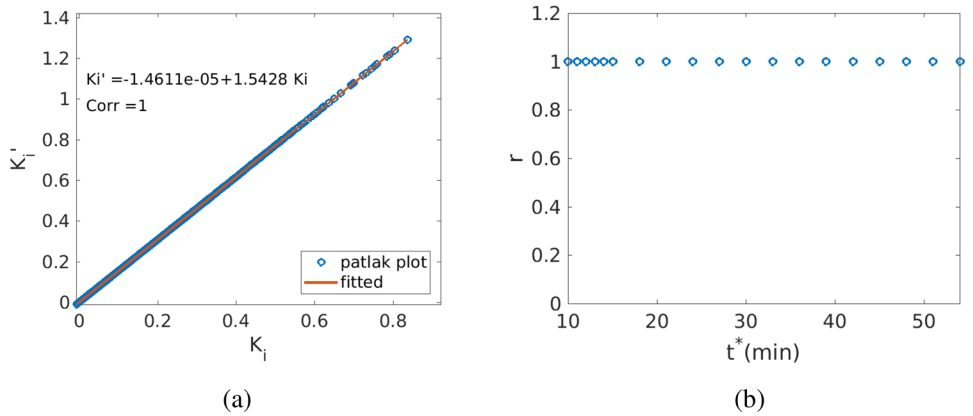

Figure 3. Results of simulation. (a) Relation between K_i' and K_i; (b) correlation coefficient of K_i' versus K_i for various t^* values.

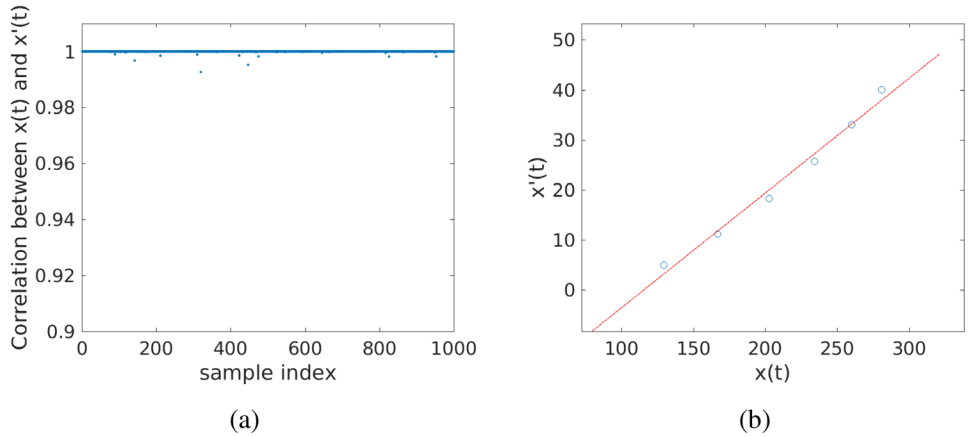

Figure 4. Validation of the approximate linear relationship between $x(t)$ and $x'(t)$ for the bi-exponential input function $C_P(t) = a_1e^{-a_2t} + b_1e^{-b_2t}$. $t^* = 30$ min. (a) Plot of the correlation coefficient of $x(t)$ versus $x'(t)$ for 1000 realizations; (b) correlation plot for a specific parameter set that corresponds to the sample point with the lowest correlation coefficient in (a).

4.2.2. Breast patient result

The parametric maps of K_i by the standard Patlak model and K_i' by the relative Patlak model with $t^* = 30$ min are shown in figure 8 for transverse, sagittal and coronal planes. The standardized uptake value (SUV) images by the static scan at 55–60 min are also included for a comparison with parametric imaging. The two parametric images have different absolute values but they appear to be proportional to each other. Compared with the SUV images, the K_i and K_i' images demonstrated higher contrast in the breast tumor region.

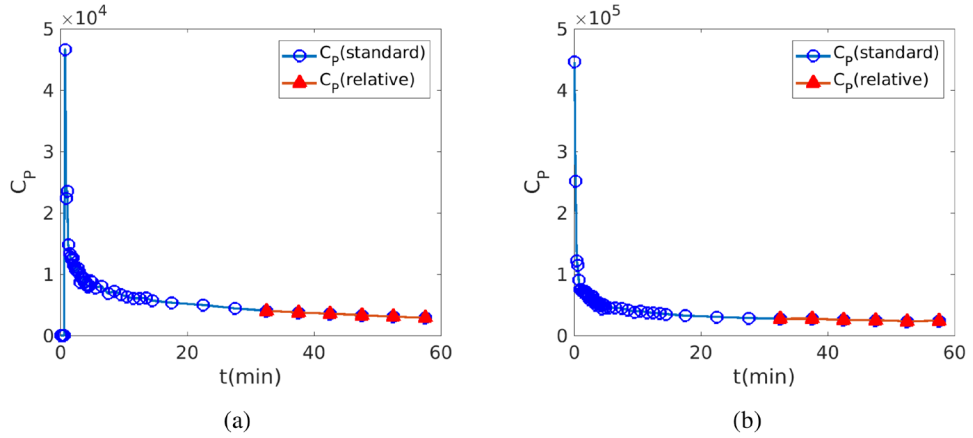

Figure 5. Blood input functions from dynamic FDG-PET scans of human patients. (a) Breast cancer patient; (b) cardiac patient.

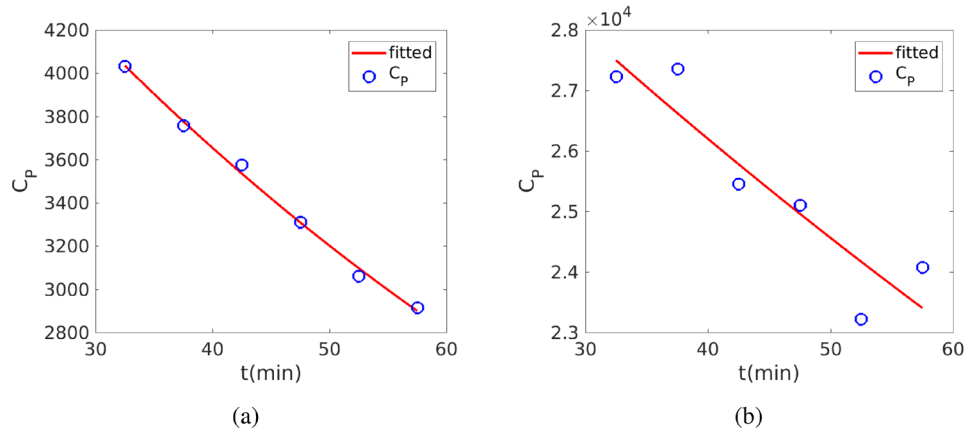

Figure 6. Validation that late-time points of real patient blood input functions approximately follow a mono-exponential function model. (a) Breast patient data, (b) cardiac patient data.

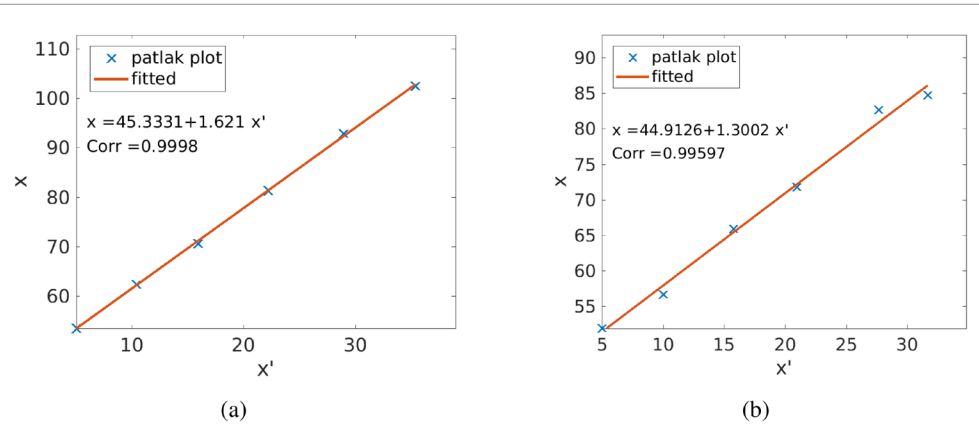

Figure 7. Linear relation between $x(t)$ and $x'(t)$ for patient data with $t \geqslant t^* = 30$ min. (a) Breast patient data, (b) cardiac patient data.

The plot of K_i' versus K_i is shown in figure 9(a). It is clear that K_i' was linearly related to K_i with a slope of 1.6199 and intercept of 1.7345×10^{-7}. The intercept was negligible so the linear relation was simply a scaling. The slope of the linear plot of K_i' versus K_i is very close to the slope of the linear plot of $x(t)$ versus $x'(t)$. The correlation coefficients between K_i' and K_i was close to 1. Figure 9(b) further shows the correlation coefficient between K_i' and K_i versus various t^* values ranging from 10 min to 50 min. High correlation remains between K_i' and K_i.

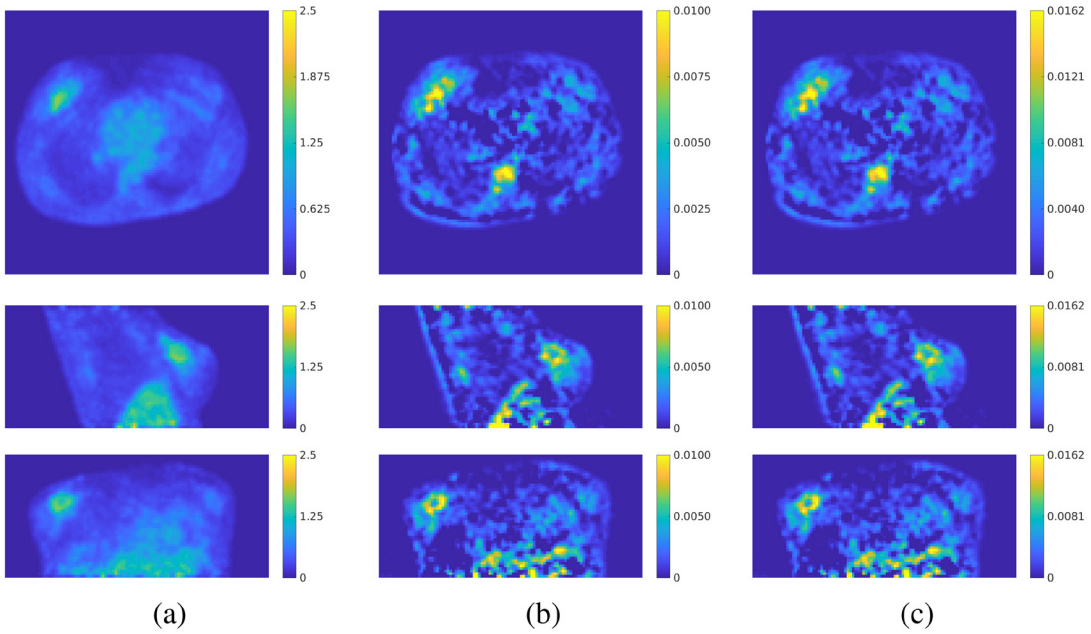

Figure 8. Comparison of SUV images and parametric imaging using the standard Patlak plot and relative Patlak plot for the breast patient. (a) SUV images; (b) parametric image of the standard Patlak slope K_i; (c) parametric image of the relative Patlak slope K_i'. The start time $t^* = 30$ min. From the top to the bottom are the views from the planes of transverse, sagittal and coronal, respectively.

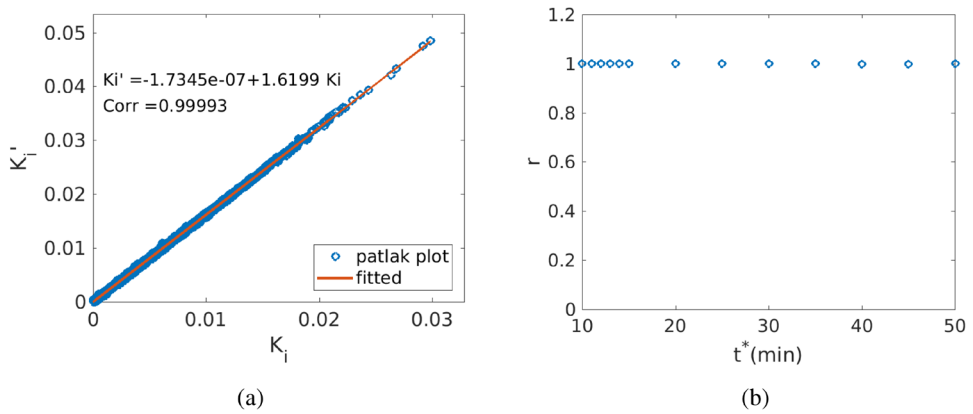

Figure 9. Results of the breast patient scan. (a) Relation between K_i' and K_i ($t^* = 30$ min); (b) correlation coefficient between K_i' and K_i versus various start time t^*.

4.2.3. *Cardiac patient result*

The SUV images of the last frame (55–60 min), parametric maps of K_i by the standard Patlak model and K_i' by the relative Patlak model with $t^* = 30$ min are shown in figure 10. Again, the two parametric images appear to be proportional to each other, though with different absolute values. The contrast of the myocardium over the blood pool is higher in the parametric images than in the SUV images.

The plot of K_i' versus K_i is shown in figure 11(a). It is again clear that K_i' is linearly related to K_i with a slope of 1.2898 and intercept of 7.7×10^{-6}. The negligible intercept indicates that the linear relation is a scaling. The slope between K_i' versus K_i is very close to the slope between $x(t)$ versus $x'(t)$ shown in figure 7(b). The correlation coefficients between K_i' and K_i and between $x(t)$ and $x'(t)$ are close to 1.

The correlation coefficient between K_i' and K_i is further plotted versus the start time t^* in figure 11(b). The correlation coefficient values remain above 0.90, though the one at $t^* = 45$ min is slightly lower then others. This can be explained by the fact in figure 7(b) that the linear correlation between x and x' for $t^* = 45$ min (i.e. the last three points) is relatively weaker, possibly due to higher noise in the cardiac scan. The corresponding K_i and K_i' images for $t^* = 45$ min are shown in figure 12. Overall, the two images still have very similar contrast appearance, indicating the scaling relation between K_i and K_i'.

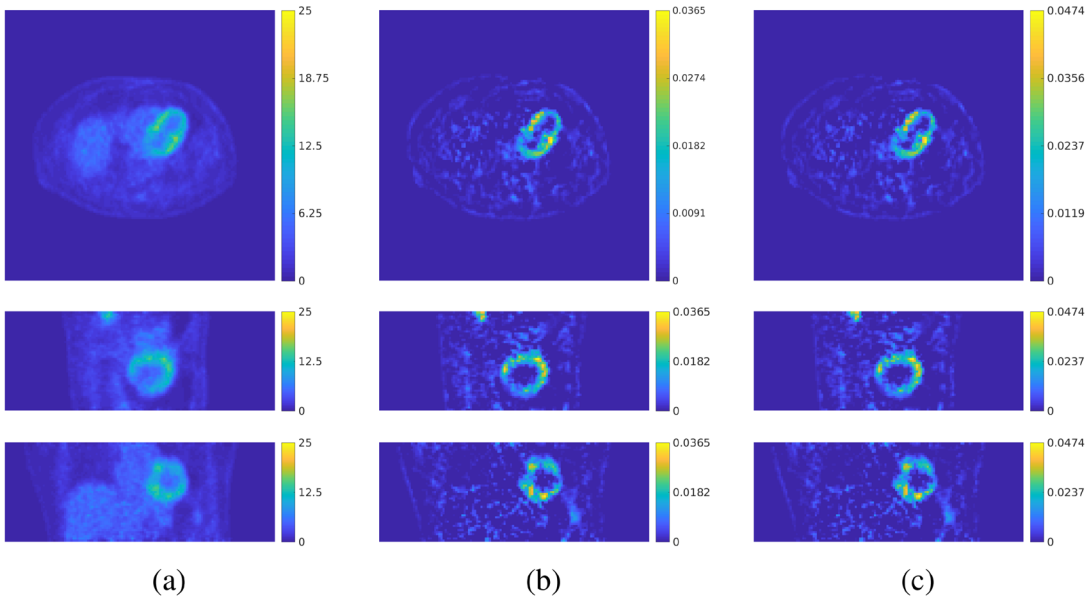

Figure 10. Comparison of SUV images and parametric imaging using the standard Patlak plot and relative Patlak plot for the cardiac patient. (a) SUV images; (b) parametric image of K_i; (c) parametric image of K_i'. The start time $t^* = 30$ min. From the top to the bottom are the views from the planes of transverse, sagittal and coronal, respectively.

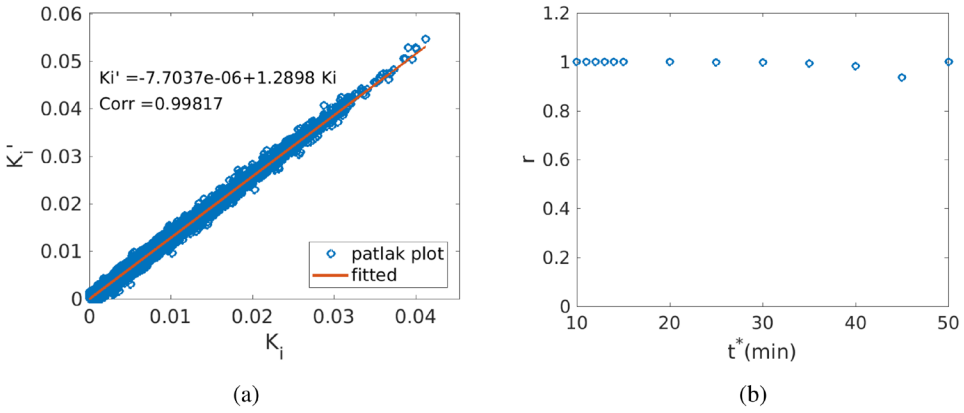

Figure 11. Results of the cardiac patient scan. (a) Relation between K_i' and K_i ($t^* = 30$ min); (b) correlation coefficient between K_i and K_i' versus various t^* values.

5. Discussion

The relative Patlak plot is a simplified version of the standard Patlak plot but brings significant advantages for practical use. The theoretical relation between the standard Patlak plot and relative Patlak plot was derived based on the assumption that the tail of a blood input function follows a mono-exponential decay model or meets an approximate linear relation between $x(t)$ and $x'(t)$. This assumption is valid in many dynamic PET scans, as demonstrated in this work by using the popular Feng input model and two blood input functions extracted from real patient data. Even if the tail of a blood input function mathematically follows a more complex model (e.g. a bi-exponential decay model) for accurate description, we have demonstrated that the relation of $x(t)$ versus $x'(t)$ can remain highly linear.

The relative Patlak plot has limitations. Compared with quantitative K_i estimates by the standard Patlak plot, a disadvantage of the relative Patlak plot is that the slope K_i' is not fully quantitative as the information of $s^* = \int_0^{t^*} C_P(\tau)dt$ is lost and the global scaling factor cannot be determined. In this regard, we do not recommend the use of K_i' as a replacement for quantitative K_i because the variability in K_i' can be different from patient to patient and from scan to scan. For example, the scaling factor was 1.6199 in the breast cancer patient and 1.2898 in the cardiac patient in the patient study. Hence, the relative Patlak plot is not directly suitable for those applications that require absolute quantification of K_i.

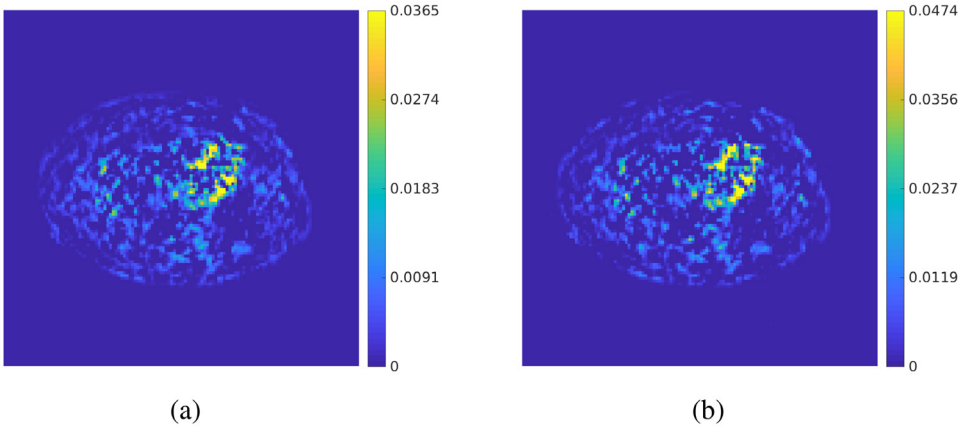

Figure 12. Parametric images of K_i and K_i' estimated with $t^* = 45$ min for the cardiac patient data. (a) K_i by the standard Patlak plot; (b) K_i' by the relative Patlak plot.

However, there are many applications that do not require absolute quantification but utilize the contrast information in the parametric image of K_i. Examples include, but are not limited to, lesion detection (e.g. Li *et al* (2009) and Yang *et al* (2016)), and metabolic tumor volume segmentation (e.g. Visser *et al* (2008)) using parametric map of tracer influx rate. The target-to-background contrast is often higher in the parametric images than in the SUV images, implying that parametric imaging can offer higher lesion detectability and better boundary differentiation (figures 8 and 10). Texture analysis based on parametric images may also provide new insight into tumor heterogeneity beyond the analysis on SUV images. In addition, for cancer imaging, a background region (e.g. the liver) may be defined to normalize the parametric image of the relative Patlak slope, then the global scaling factor can be removed. The normalized K_i' is quantitatively equal to the normalized K_i and can be used for quantitative monitoring in a longitudinal study. We will investigate the feasibility of normalized K_i' for this purpose in a future patient study.

The investigation and development in this work are also timely because recently whole-body Patlak parametric image reconstruction has become available in commercial PET scanners (Hu *et al* 2017). The new relative Patlak plot can have a clear impact on practical use.

6. Conclusion

We propose a new relative Patlak plot method for analyzing dynamic PET data. The new plot excludes the need for early-time input function and only requires late-time input function data, thus is easier to use than the standard Patlak method. Theoretical analysis, simulation results and real patient data all have demonstrated that parametric imaging by the relative Patlak plot determines the parametric image of the standard Patlak slope up to a global scaling factor. The new relative plot can replace the standard Patlak plot for certain applications where the determination of the global scaling factor is not necessary, such as lesion detection, metabolic volume segmentation, and texture analysis.

Acknowledgments

The authors thank the reviewers for helpful comments. The work is supported in part by NIH under no. R21 HL 131385 and by AHA under no. BGIA 25780046. GW is also supported in part by the UC Davis Comprehensive Cancer Center under NIH grant no. P30 CA093373 and K12 CA138464.

ORCID iDs

Jinyi Qi https://orcid.org/0000-0002-5428-0322
Guobao Wang https://orcid.org/0000-0001-6526-1533

References

Angelis G I, Thielemans K, Tziortzi A C, Turkheimer F E and Tsoumpas C 2011 Convergence optimization of parametric mlem reconstruction for estimation of patlak plot parameters *Comput. Med. Imaging Graph.* **35** 407–16

Choi Y, Hawkins R A, Huang S C, Gambhir S S, Brunken R C, Phelps M E and Schelbert H R 1991 Parametric images of myocardial metabolic-rate of glucose generated from dynamic cardiac pet and 2- f-18 fluoro-2-deoxy-d-glucose studies *J. Nucl. Med.* **32** 733–8

Choi Y, Huang S C, Hawkins R A, Kuhle W G, Dahlbom M, Hoh C K, Czernin J, Phelps M E and Schelbert H R 1993 A simplified method for quantification of myocardial blood-flow using nitrogen-13-ammonia and dynamic pet *J. Nucl. Med.* **34** 488–97

Feng D, Huang S C and Wang X M 1993 Models for computer-simulation studies of input functions for tracer kinetic modeling with positron emission tomography *Int. J. Bio-Med. Comput.* **32** 5–110

Gambhir S S, Schwaiger M, Huang S C, Krivokapich J, Schelbert H R, Nienaber C A and Phelps M E 1989 Simple noninvasive quantification method for measuring myocardial glucose-utilization in humans employing positron emission tomography and f-18 deoxyglucose *J. Nucl. Med.* **30** 359–66

Gill S S, Patel N K, Hotton G R, O'Sullivan K, McCarter R, Bunnage M, Brooks D J, Svendsen C N and Heywood P 2003 Direct brain infusion of glial cell line-derived neurotrophic factor in parkinson disease *Nat. Med.* **9** 589–95

Gunn R N, Sargent P A, Bench C J, Rabiner E A, Osman S, Pike V W, Hume S P, Grasby P M and Lammertsma A A 1998 Tracer kinetic modeling of the 5-ht1a receptor ligand carbonyl-c-11 way-100635 for pet *Neuroimage* **8** 426–40

Hackstein N, Bauer J, Hauck E W, Ludwig M, Kramer H J and Rau W S 2003 Measuring single-kidney glomerular filtration rate on single-detector helical ct using a two-point patlak plot technique in patients with increased interstitial space *Am. J. Roentgenol.* **181** 147–56

Hackstein N, Wiegand C, Rau W S and Langheinrich A C 2004 Glomerular filtration rate measured by using triphasic helical ct with a two-point patlak plot technique *Radiology* **230** 221–6

Hom J, Dankbaar J W, Schneider T, Cheng S C, Bredno J and Wintermark M 2009 Optimal duration of acquisition for dynamic perfusion ct assessment of blood–brain barrier permeability using the patlak model *Am. J. Neuroradiol.* **30** 1366–70

Hu J, Panin V, Smith A M, Vijay Shah W H, Kehren F and Casey M 2017 Clinical whole body CBM parametric PET with flexible scan modes *Conf. Record of IEEE Nuclear Science Symp. and Medical Imaging Conf.* (https://www.eventclass.org/contxt_ieee2017/online-program/session?s=M-08#2146)

Karakatsanis N A, Casey M E, Lodge M A, Rahmim A and Zaidi H 2016 Whole-body direct 4D parametric PET imaging employing nested generalized Patlak expectation-maximization reconstruction *Phys. Med. Biol.* **61** 5456–85

Karakatsanis N A, Zhou Y, Lodge M A, Casey M E, Wahl R L, Zaidi H and Rahmim A 2015 Generalized whole-body Patlak parametric imaging for enhanced quantification in clinical PET, *Phys. Med. Biol.* **60** 8643–73

Kordower J H *et al* 2000 Neurodegeneration prevented by lentiviral vector delivery of GDNF in primate models of parkinson's disease *Science* **290** 767–73

Li Z, Li Q, Yu X, Conti P S and Leahy R M 2009 Lesion detection in dynamic FDG-PET using matched subspace detection *IEEE Trans. Med. Imaging* **28** 230–40

Miles K A, Leggett A C D and Bennett A J G 1999 CT derived patlak images of the human kidney *Br. J. Radiol.* **72** 153–8

Patlak C S and Blasberg R G 1985 Graphical evaluation of blood-to-brain transfer constants from multiple-time uptake data—generalizations *J. Cerebral Blood Flow Metab.* **5** 584–90

Patlak C S, Blasberg R G and Fenstermacher J D 1983 Graphical evaluation of blood-to-brain transfer constants from multiple-time uptake data *J. Cerebral Blood Flow Metab.* **3** 1–7

Rahmim A, Tang J and Zaidi H 2009 Four-dimensional (4D) image reconstruction strategies in dynamic PET: beyond conventional independent frame reconstruction *Med. Phys.* **36** 3654–70

Reader A J and Verhaeghe J 2014 4D image reconstruction for emission tomography *Phys. Med. Biol.* **59** R371–418

Schmidt K C and Turkheimer F E 2002 Kinetic modeling in positron emission tomography *Q. J. Nucl. Med.* **46** 70–85 (https://www.minervamedica.it/en/journals/nuclear-med-molecular-imaging/article.php?cod=R39Y2002N01A0070)

Tang J, Kuwabara H, Fwong D and Rahmim A 2010 Direct 4d reconstruction of parametric images incorporating anato-functional joint entropy *Phys. Med. Biol.* **55** 4261–72

Tsoumpas C, Turkheimer F E and Thielemans K 2008 Study of direct and indirect parametric estimation methods of linear models in dynamic positron emission tomography *Med. Phys.* **35** 1299–309

Visser E P, Philippens E P M, Kienhorst L, Kaanders J, Corstens H M F, de Geus-Oei L F and Oyen J G W 2008 Comparison of tumor volumes derived from glucose metabolic rate maps and suv maps in dynamic f-18-FDG PET *J. Nucl. Med.* **49** 892–8

Wang G B, Fu L and Qi J Y 2008 Maximum *a posteriori* reconstruction of the patlak parametric image from sinograms in dynamic PET *Phys. Med. Biol.* **53** 593–604

Wang G B and Qi J Y 2013 Direct estimation of kinetic parametric images for dynamic PET *Theranostics* **3** 802–15

Wu Y and Carson R E 2002 Noise reduction in the simplified reference tissue model for neuroreceptor functional imaging *J. Cerebral Blood Flow Metab.* **22** 1440–52

Yang L, Wang G and Qi J 2016 Theoretical analysis of penalized maximum-likelihood Patlak parametric image reconstruction in dynamic PET for lesion detection *IEEE Trans. Med. Imaging* **35** 947–56

Zhu W, Li Q, Bai B, Conti P S and Leahy R M 2014 Patlak image estimation from dual time-point list-mode PET data *IEEE Trans. Med. Imaging* **33** 913–24

Zhou Y, Sojkova J, Resnick S M and Wong D F 2012 Relative equilibrium plot improves graphical analysis and allows bias correction of standardized uptake value ratio in quantitative ^{11}C-PiB PET studies *J. Nucl. Med.* **53** 622–8